CHAPTER 7

Radiofrequency Finger Augmentation Devices for the Tactile Internet

G. M. Bianco and G. Marrocco

7.1 Introduction

The tactile internet (TI) is an emerging technology consisting of extremely low-latency systems with tactile inputs and audio/video feedback [1]. A maximum round-trip delay of about 1 ms is required not to have the users suffer from cybersickness [2, 3], and enable applications ranging from exoskeleton controlling to remote driving. Figure 7.1(a) shows the evolution from the mobile internet to the TI and their main features. The ultimate goal of the TI is the remote delivery of physical senses through the internet, creating the internet of skills [4] that merges the TI with artificial intelligence to achieve the perception of zero-delay networks. Although the 5G network can enable new body-centric communication networks, the TI is still in its infancy. The implementation of TI systems still needs research concerning the physical layer, resource management and networking issues, as well as the combined use of different protocols [5].

A 5G hand-worn system capable of capturing the human tactile experience has yet to be developed, although progress can come from finger augmentation devices (FADs), which are defined as "finger-worn devices with an additional augmentation other than their form, that provide a supplemental capability for one or more fingers using the finger itself as a central element" [6]. Two examples of FADs are an on-nail display [7] and a touch-sensitive pad [8]. The main limitation of FADs is their powering since wires hinder any free-hand gestures, resulting in discomfort for the wearer. Instead, wireless FADs usually are paired with an off-body companion device, and the resulting system is not wearable as a whole [6]. More comfortable fingertip devices can be fabricated by resorting to epidermal electronics, which are ultrathin, soft electronics adhering directly onto the human skin and mechanically imperceptible for the user [9]. The on-body powering issue was overcome by combining FADs with the RFID paradigm, creating a new class of systems named radiofrequency finger augmentation devices (R-FADs).

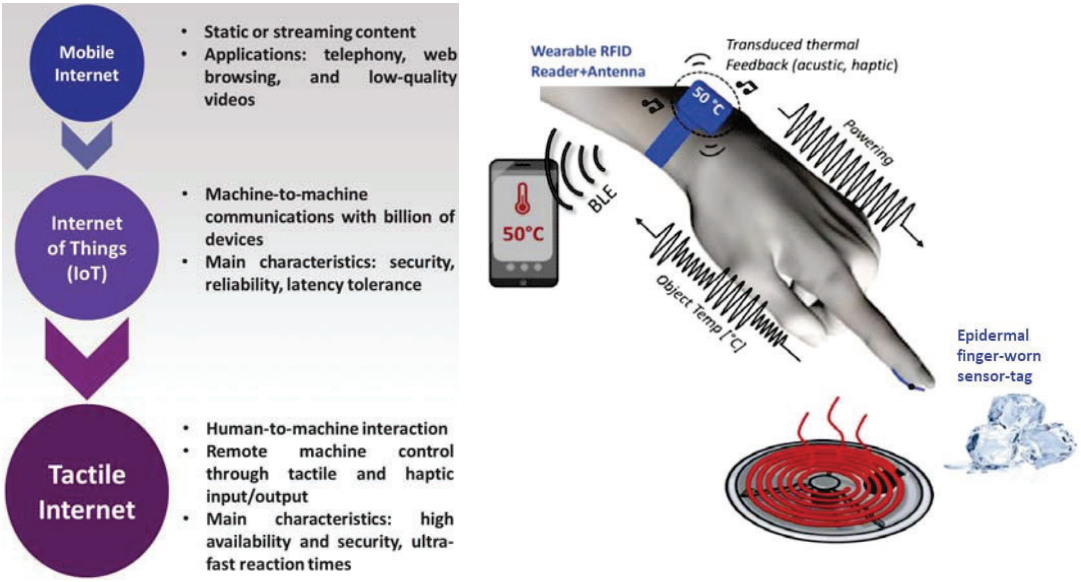

Figure 7.1 (a) Leaps of the tactile internet. (Adapted from [5].) (b) Sketch of R-FADs for temperature-sensing. (© 2019 IEEE [16].)

Although many RFID-based FADs were proposed (e.g., [10–13]), the term R-FAD here specifically refers to a system composed of finger-worn sensors provided with sensing capabilities that communicate with a reader antenna placed on the wrist. The system is powered by a portable reader source that utilizes a processing unit to give feedback to the user (Figure 7.1(b)). The EM wave generated by the reader's antenna energizes the fingertip sensor, which, in turns, modulates and backscatters the wave toward the reader. In this way, there is no wire connected to the fingertips, the system is wholly wearable, and natural free-hand gestures are preserved. Current R-FADs communicate through UHF (860–960 MHz) links, and their latency is higher than 1 ms as required by TI applications. Nonetheless, the ongoing research on 5G RFID systems [14] allows envisaging 5G R-FADs in the near future. While the 5G technology becomes more mature, current UHF R-FADs can be exploited in the short term to test and study the wrist-finger links through backscattering modulation.

R-FADs have recently been tested to recover thermal sensitivity, which can be lost because of life-saving medical treatments and is vital to perform everyday activities, like cooking, without suffering injuries. R-FAD systems can also provide the wearer with sensorial ultrability. R. Shilkrot in [15] first used this term to describe new types of perception not inherent to the natural human capabilities and obtained through an artificial interface. As a practical example, the dielectric-sensing R-FAD can provide the wearer with the ultrability of sensing the electric permittivity of the material being touched.

This ultrability is obtained through a recently introduced class of self-tuning integrated circuits (ICs) that can automatically modify their internal impedance to make the matching to the hosting antenna nearly insensitive to changes in local boundary conditions.

This chapter reviews the state of the art on R-FADs concerning the following topics:

1. Communication models for the fingertip-wrist backscattering link and its variability;
2. Design method for fingertip RFID dielectric sensors;
3. Epidermal flexible and stretchable devices for transforming our fingertips into touch scanners;
4. Applications of R-FADs to aid sensorially impaired people;
5. Digital therapy for studying the cognitive remapping applied to the lost thermal feeling.

7.2 Communication Models for the Fingertip-Wrist Backscattering Link and Its Variability

The wrist-worn reader communicates via backscattering with the fingertip sensors in the R-FAD architecture. Thus, the EM challenge consists of establishing a robust fingertip-wrist link in the presence of the lossy human body and during natural gestures. Reference [17] introduces and analyzes the wrist-finger links. There are several challenges in establishing such links.

1. Since a wearable battery-fed reader is needed for a fully wearable R-FAD, the available power is reduced with respect to a fixed interrogation station;
2. The direct contact between the antennas and the wearer's skin generates high power losses;
3. The wrist-finger channel is significantly time-variant due to the free-hand gestures, which continuously change the mutual arrangement of antennas;
4. The EM interactions occur near both the antennas and the human body;
5. Multiple sensors can be used simultaneously; hence the intersensor coupling could further complicate the interaction.

Since the antennas' arrangements are dependent on the morphology of the user's hand and on the gesture performed, the link is characterized by intersubject (user-dependent) and intrasubject (no user-dependent) variabilities.

The complex wrist-finger communication operates in the midfield and can be analyzed through a two-port model (Figure 7.2(a)) that accounts for everything between the reader's antenna feeding port and the IC. The lossy two-port network is characterized by its 2×2 impedance (Z), admittance (Y), or scattering (S) matrix. The antennas are represented through their Thevenin (Z-, S-matrix) or Norton (Y-matrix) equivalent circuits. The metric to characterize the links is the transducer power gain (G_T), defined as the ratio between the power $P_{R \to T}$ delivered by the reader to the chip in the specific impedance matching condition and the available power emitted by the reader generator $P_{av,R}$. By assuming a two-port network characterized through the impedance Z-matrix, the G_T can be evaluated as [19]

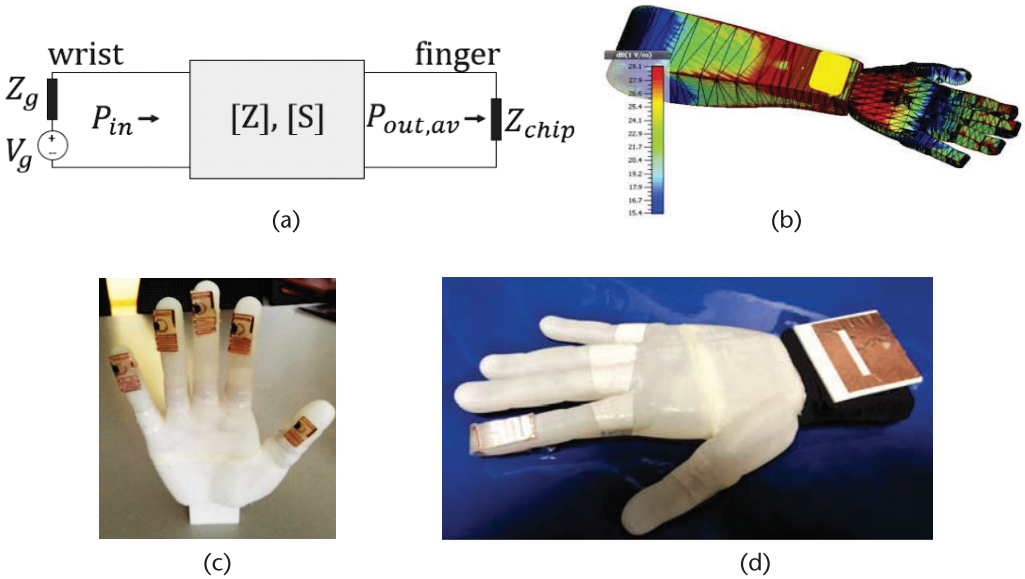

Figure 7.2 (a) Two-port model of the wrist-finger link. (© 2019 IEEE [17].) (b) Homogeneous numerical hand phantom and E-field when a wrist patch (yellow rectangle) is active and fed with 1W source power. (© 2017 IEEE [18].) A 3-D-printed hand phantom equipped with (c) five finger sensors and (d) an R-FAD prototype with both the antennas of the sensor and the reader. (© 2017 IEEE [18].)

$$G_T = \frac{P_{R\to T}}{P_{av,R}} = \frac{4R_{IC}R_G\left|Z_{21}\right|^2}{\left|\left(Z_{11}+Z_G\right)\left(Z_{22}+Z_{IC}\right)-Z_{12}Z_{21}\right|^2} \tag{7.1}$$

where $Z_{IC} = R_{IC} + \mathrm{j}X_{IC}$ is the microchip impedance, and $Z_G = R_G + \mathrm{j}X_G$ is the generator impedance. Similarly, the G_T can be evaluated by the admittance Y-matrix [20]

$$G_T = \frac{4G_{IC}G_G\left|Y_{21}\right|^2}{\left|\left(Y_{11}+Y_G\right)\left(Y_{22}+Y_{IC}\right)-Y_{12}Y_{21}\right|^2} \tag{7.2}$$

where $Y_{IC} = Y_{IC} + \mathrm{j}B_{IC}$ is the chip admittance, and $Y_G = G_G + \mathrm{j}B_G$ is the generator admittance. In the ideal case of perfect impedance matching at both ports, G_T is maximum and it is called system power gain (g), which can be evaluated from the scattering S-matrix [21]

$$g = \frac{\left|S_{21}\right|^2}{\left(1-\left|S_{11}\right|^2\right)\left(1-\left|S_{22}\right|^2\right)} \tag{7.3}$$

The system power gain is usually employed to study the phenomenology of fingertip-wrist communications through numerical simulations[1] and to evaluate the optimum achievable link performance.

1. The numerical phantoms and the EM simulations in this chapter were obtained by CST® Microwave Studio 2018.

All the numerical analyses hereafter reviewed consider a reference R-FAD and a homogeneous hand phantom (Figure 7.2(b)). First, the feasibility of energizing R-FAD devices through a portable reader was numerically evaluated, accounting for the power losses caused mainly by the hand [17]. Let P_{IC} be the IC sensitivity (i.e., the minimum power needed by the IC to activate and interact with the reader) in dBm, and p_S an arbitrary safety margin accounting for the uncertain knowledge of the IC and the limited control on the actual power emitted by the reader. The analysis of the link also considers a set of M known hand gestures. The minimum input power P_{in} required to activate the communication in the overall set of considered gestures is, then,

$$P_{in,min} = \frac{p_{IC} + p_S}{\min\limits_{1 \le m \le M} \{g_m\}} \tag{7.4}$$

Body-worn R-FADs have been extensively numerically analyzed in [17] concerning bending, SAR, link quality when performing different gestures, and intersensor coupling. First, the fingertip sensor impedance match is not significantly affected by bending or hand gestures. Similarly, when considering a wrist-mounted patch as the reader's antenna, the H-plane bendings are negligible [22]. Regarding the SAR, the R-FAD causes minimal power absorption. When sourcing an R-FAD reader by 1W of input power, the wrist-mounted patch generates a SAR of 9 mW/kg, which is significantly lower than the EU regulation of 4 W/kg.

Concerning the intrasubject variability due to different gestures, differences in the g of about 15 dB are observed between the best-case and the worst-case gestures. This difference also depends on the sensor antenna layout. Finally, if multiple fingertip sensors are worn simultaneously, the strong power absorption by the human tissues causes the on-finger antennas to be negligibly EM coupled. Accordingly, the six-port equivalent model of the multichannel R-FAD can be reduced to five equivalent two-port networks, each representing a reader-tag link.

In [18], the first R-FAD prototype was tested on a 3-D-printed hand model, filled with a liquid reproducing the human body electric properties (Figure 7.2(c,d)). When evaluating the same link multiple times by removing and repositioning the sensor, the measured G_T experiences some fluctuations due to the different adherence to the hand phantom. Thus, sensor prototypes ensuring a reproducible and stable adherence are required to obtain a highly reliable link.

Based on the mathematical formulation in (7.4), simulations revealed that a value of $P_{in,min} \le 27$ dBm allows establishing a robust link over three common gestures (hand open, index touching, and prehension) [17]. Accordingly, a commercially available RFID portable reader can successfully power R-FAD systems. The first R-FAD prototype tested on real users is shown in Figure 7.3(a). The different sensor-reader links for each finger were measured to assess the intrasubject variability of the R-FAD communications due to the specific channels. A maximum difference of 5 dB in the measured G_T for a given gesture and user was observed [17]. Statistical analysis was performed on 10 different users (the hand form-factors in Figure 7.3(b)) wearing the sensor on the index finger, and each performing five given gestures (Figure 7.3(c)). The evaluated maximum difference was 13 dB (Fig-

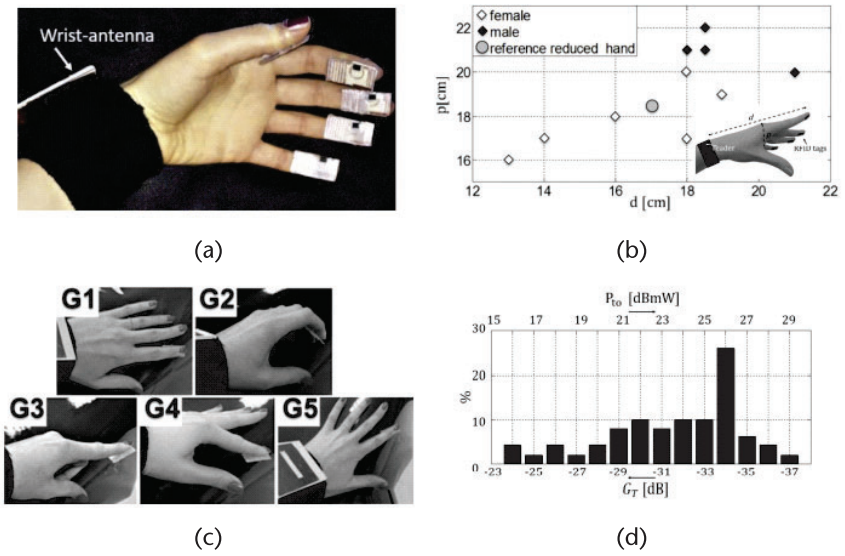

Figure 7.3 (a) Multisensor R-FAD prototype worn by a volunteer. (© 2019 IEEE [17].) (b) Hand sizes of the test population. (© 2019 IEEE [17].) (c) Five gestures performed by each volunteer of the test population. (© 2019 IEEE [17].) (d) Normalized distribution of Gt at 870 MHz of the R-FAD for all the considered volunteers and hand gestures and corresponding Pto in the case of Pic = –5 dBm. (© 2019 IEEE [17].)

ure 7.3(d)), but a portable reader emitting 27 dBm can still energize the single-worn sensor in 95% of the considered combinations anyway [17].

7.3 Constrained Design of R-FADs

When wearing an R-FAD during the day, the user may have to interact with multiple objects and materials. During the interactions, the environment where the sensor operates changes, and the consequent impedance mismatch between the fingertip antenna and the IC can compromise the wrist-finger link and prevent any communication. Accordingly, the design of the R-FADs will be constrained to make the on-hand link reliable independent of the interactions performed by the wearer. This reliability is possible by resorting to temperature-sensing ICs capable of autotuning (also known as self-tuning; an example of such microchips is the Magnus S3 by Axzon).

Autotuning ICs are capable of modifying their internal impedance to compensate for changes in the boundary conditions. They can be modeled as a resistance in parallel to a variable capacitance, which in turn can be considered as a switchable ladder of equal capacitors of capacitance C_0 so that the IC overall capacitance is $Cic(n) = Cmin + nC_0$ [23]. With reference to Figure 7.4(a), the number n of equal equivalent capacitors to compensate for the admittance $Y_T(\psi)$,which depends on the boundary conditions ψ seen by the IC, is determined by the self-tuning equation [23]:

$$\left|B_{IC}(n) + B_T(\psi)\right| = 0 \tag{7.5}$$

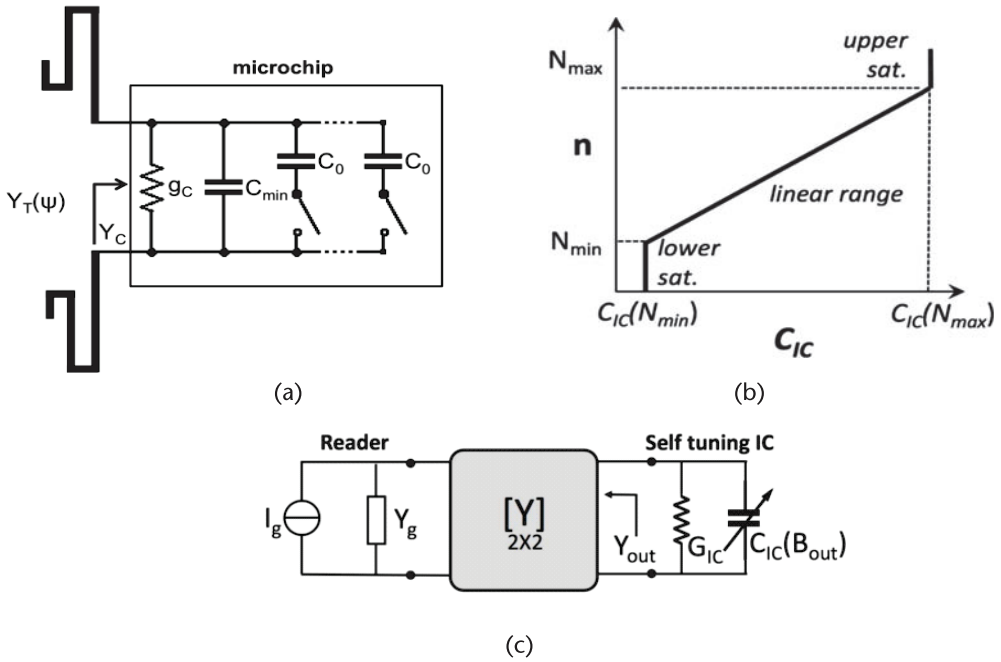

Figure 7.4 (a) Equivalent circuit of an autotuning IC. (© 2018 IEEE [23].) (b) Lower and upper saturation zones of an autotuning IC, and linear range wherein the self-tuning equation holds. (© 2020 IEEE [24].) (c) Two-port model of a wrist-finger link including an autotuning IC. (© 2020 IEEE [24].)

where $B_T(\psi) = \mathrm{Im}[Y_T(\psi)]$, $B_{IC}(n) = 2\pi f C_{IC}(n)$, and f is the frequency. The self-tuning equation holds if n is comprised between N_{min} and N_{max}, whose values depend on the actual IC considered. If $n \leq N_{min}$ or $n \geq N_{max}$, saturation occurs (Figure 7.4(b)) [24]. The tuning parameter n is also returned by the IC to the reader through a metric called sensor code (SC). The SC can be exploited for sensing, too, as shown next in Section 7.5.2.

When considering a self-tuning fingertip sensor, the two-port model of the wrist-finger link must account for the variable IC capacitance (Figure 7.4(c)) The model can be employed to design finger sensors, optimizing the communication link with the reader. Let us assume that all the J expected interactions are fully characterized by a set of values $\psi = \{\psi_1, ..., \psi_J\}$ of a physical parameter ψ. As a practical example, $\psi = \varepsilon = Re(\varepsilon_C)$, where ε_C is the complex permittivity of the touched material. Then, the vector $\psi = \varepsilon = \{\varepsilon_1, ..., \varepsilon_J\}$ represents the boundary conditions wherein the fingertip sensor must work. The optimal design of the sensor must ensure a reliable wrist-finger link in the above boundary conditions and, to optimally utilize the self-tuning feature of the IC, the antenna susceptance $B_T(\psi)$ has to be exactly mapped in the linear range of the IC (Figure 7.4 (b)). With reference to the loop-matched [25] dipole layout in Figure 7.5(a), the set of geometrical parameters to be optimized is a = $\{a_1, a_2\}$. The optimization problem is formalized as the minimization of the penalty function U(**a**):

$$U(\mathbf{a}) = \sum_{i=1}^{3} w_i u_i(\mathbf{a}) \tag{7.6}$$

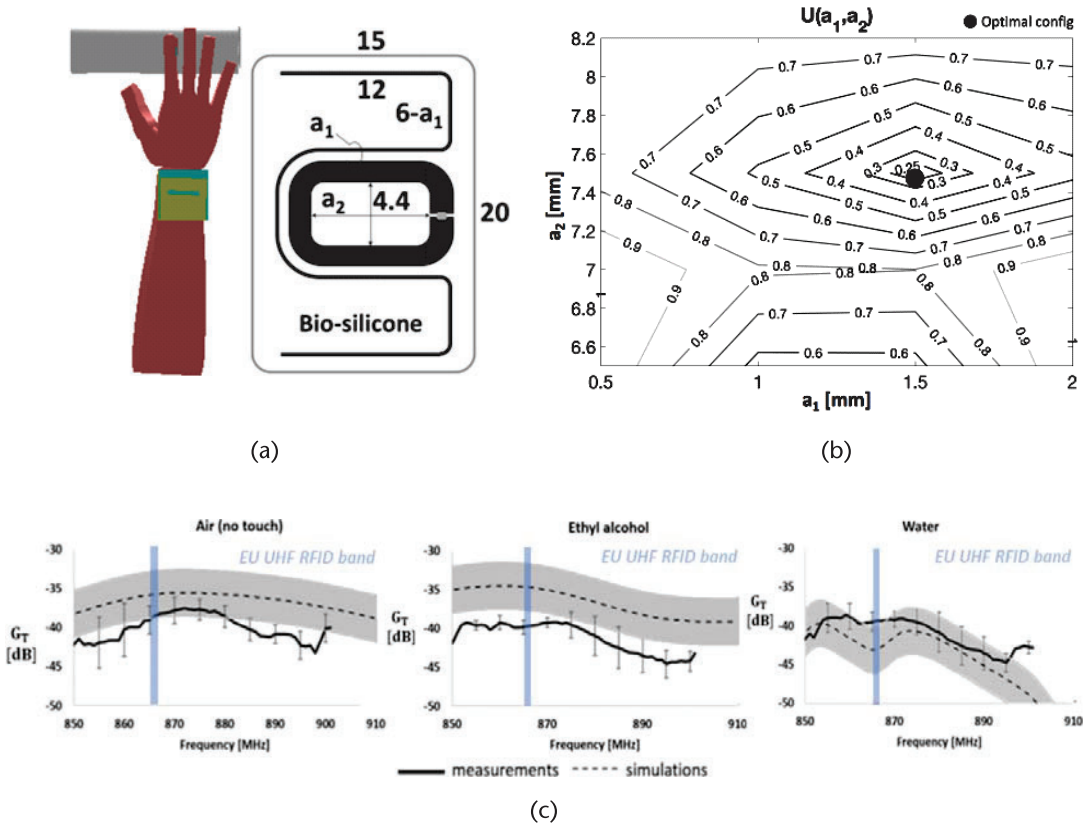

Figure 7.5 (a) Layout of a loop-matched fingertip antenna to be optimized through constrained design (left) and numerical model of the hand contacting a cylindrical container (right). (© 2020 IEEE [24].) (b) Penalty function U(a) with the indication of the optimal couplet {a1, a2}, with regard to the antenna layout in Figure 7.5(a). (© 2020 IEEE [24].) (c) Transducer power gain of the constrained-designed fingertip sensor (from Figure 7.5(a,b)) when contacting PET bottles filled with three different materials. The ±3-dB shadowed region around the simulated values account for the expected intrasubject variabilities, and the EU UHF RFID band is highlighted in blue. (© 2020 IEEE [24].)

The w_i terms are weights, whereas the three addends $u_i(\mathbf{a})$ enforce the minimization of (1) the activation power, (2) the difference $\min_{1\le j\le J}\left(n_j\right) - N_{min}$, and (3) the difference $N_{max} - \max_{1\le j\le J}\left(n_j\right)$. In this way, the communication performance is optimized and the autotuning linear range is fully exploited, thus avoiding saturation [24]. When numerically evaluating (7.6), the minimum $U(\mathbf{a})$ identifies the optimal design of the fingetip antenna (Figure 7.5(b)) that achieves stable performances in the considered variable boundary conditions.

An example with three boundary conditions (air, ethyl alcohol, and water) in a vast range of permittivities ($\varepsilon = \{1, 17, 78\}$, respectively) is shown in Figure 7.5(c). The average standard deviation in the 865.6–867.6-MHz band [26] is about just 1 dB over the three materials. Overall, the achieved performance can be considered rather insensitive to the touched item.

7.4 R-FAD Manufacturing

State-of-the-art wrist antennas in R-FADs are the folded patches, as shown in Figure 7.2(d). These antennas are worn on the wrist using cloth bracelets directly contacting the human skin (Figure 7.3(a)) and hosting the reader module as well (Figure 7.6(a)). Their substrate is a slightly stretchable low-permittivity closed-cell polyvinyl-chloride foam ($\varepsilon = 1.55$, $\sigma = 6 \cdot 10^{-4}$ S/m) [17], which can moderately bend to conform to the user's wrist morphology. The most appropriate placement of the reader's antenna when considering both the communication link and the user's comfort is the topside of the wrist [17].

The fingertip sensors have to be soft and possibly stretchable because of their positioning; otherwise, the interactions with objects will be hindered. Different kinds of finger sensors were designed, such as (Figure 7.7): (1) on-silicone sensors, (2) plaster sensors, and (3) in-silicone sensors. The first type of finger sensors is made of adhesive copper placed onto substrates of biocompatible silicone to adhere to the human skin. The copper is cut by carving machines (e.g., the Secabo S60II plotter). Examples of on-silicone sensors are the U-shaped meander-line dipole (U-tag; Figure 7.6(b)), and the flat-meandered dipole (F-tag; Figure 7.6(c)). The proximity to the human body is a critical factor when designing epidermal sensors, and millimetric differences in the antenna-body distance significantly impact the antenna's impedance parameters and, consequently, the antenna-IC impedance matching.

On-silicone sensors are moderately stretchable; they use silicone as support to be worn and can be removed and reused again. However, their limited stretchability and flexibility can be uncomfortable for the wearer, such as when grasping objects. The comfortability is greatly improved utilizing thin plaster tags [27]. The plaster tags are disposable sensors fixed onto the fingertip through self-adhering thin breathable films (Figure 7.8(a,b)). These sensors are highly flexible and non-invasive. Due to the high losses caused by the human body, a small square silicone spacer between the IC and the skin is still included to preserve the finger-wrist link. Since these epidermal sensors adhere directly to the human skin, they must follow every digit movement without breaking or degrading their performance. The adhesion is obtained by utilizing a medical tape, for example, 3M™ Tegaderm™, or Fixomull® by BSN Medical.

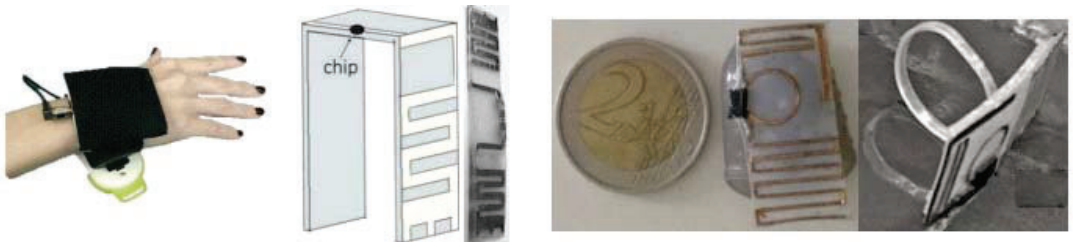

(a) (b) (c)

Figure 7.6 (a) Reader and antenna of the wrist-worn readers. (© 2019 IEEE [16].) (b) Layout and prototype of the fingertip U-tag. (© 2019 IEEE [17, 18]). (c) Two F-tag prototypes using different silicone supports. (© 2019 IEEE [17].)

Figure 7.7 Multichannel R-FAD systems employing different types of finger sensors. From left to right: on-silicone sensors, plaster-sensors, and in-silicone sensors.

Figure 7.8 Plaster-finger sensors: (a) double-phalanx antenna. (Adapted from [28].) (b) Distal phalanx antenna, designed as in Figure 7.5. (© 2020 IEEE [24].) (c) In-silicone double-phalanx finger sensors. (Tag from [29].)

In all cases, adherence is a critical issue that can affect the robustness of sensing and communication [24]. Consequently, the size of such sensors is more crucial than those of on-silicone ones since bending the fingers can cause the epidermal plaster sensors to lose adhesion to the skin. To minimize the antenna's size and mechanical stiffness, thin copper-wire antennas can be used, as the loop-matched dipole in Figure 7.8(b). Such thin-wire epidermal antennas suffer from degradation in their radiation performance if excessively stressed for longer than a day [30]. This is not expected to happen with disposable plaster sensors due to their limited use time. Because of hand movements, small sensors placed on a single phalanx (Figure 7.8(b)) are more effective than utilizing antennas covering both the intermediate and the distal phalanxes (Figure 7.8(a)), even if double-phalanx antennas can achieve better radiation performance thanks to the broader available surface. In any case, due to the submillimetric plaster and the thin copper dipole, this second type of sensor gets damaged when removed from the fingertip and cannot be reused.

Finally, in-silicone epidermal fingertip antennas manage to preserve both the reusability of the on-silicone sensors and the stretchability and comfort of the plaster sensors. The in-silicone sensors consist of an antenna embedded within ultrathin elastomeric layers that protect the antenna and simultaneously adheres to the human skin (Figure 7.8(c)). The antenna layout is the same as the plaster sensors in Figure 7.8(a), whereas the embedding silicone is composed of two different stretchable silicone components having different Young's moduli (Figure 7.9(a)). Two Ecoflex™ 00-30 (by Smooth On; thickness ~0.3 mm each) layers embed the antenna, and one layer of Silbione™ (by Elkem Silicones; thickness ~0.1 mm) fixes the sensor onto the finger's skin (Figure 7.9(b,c)). The Silbione™ layer allows the epidermal antenna to follow the finger movements even in the case of double-phalanx sensors, like those in Figure 7.8(c). In-silicone sensors are highly flexible, have a total thickness lower than 1 millimeter, and can easily be removed, cleaned, sanitized, and reapplied on the finger several times.

7.5 R-FAD Applications to Aid Sensorially Impaired People

The R-FAD systems were initially proposed to aid people suffering from hypoesthesia (i.e., a sensory impairment resulting in a reduction of sensitivity to specific kinds of stimuli). In particular, R-FADs can be used as soft tools to permanently overcome thermal and tactile hypoesthesia, as well as visual impairment. Thermal and tactile hypoesthesia are usually symptoms of peripheral neuropathy [31], a common disorder that is increasingly widespread due to obesity and aging and can incidentally be caused by many pathologies and medical treatments, like sickle cell disorder [32], diabetic neuropathy [33], or chemotherapy [34]. Sensorially impaired individuals incur several issues during daily activities, like getting severely burned without noticing. Regarding visual impairments, 285 million people were estimated

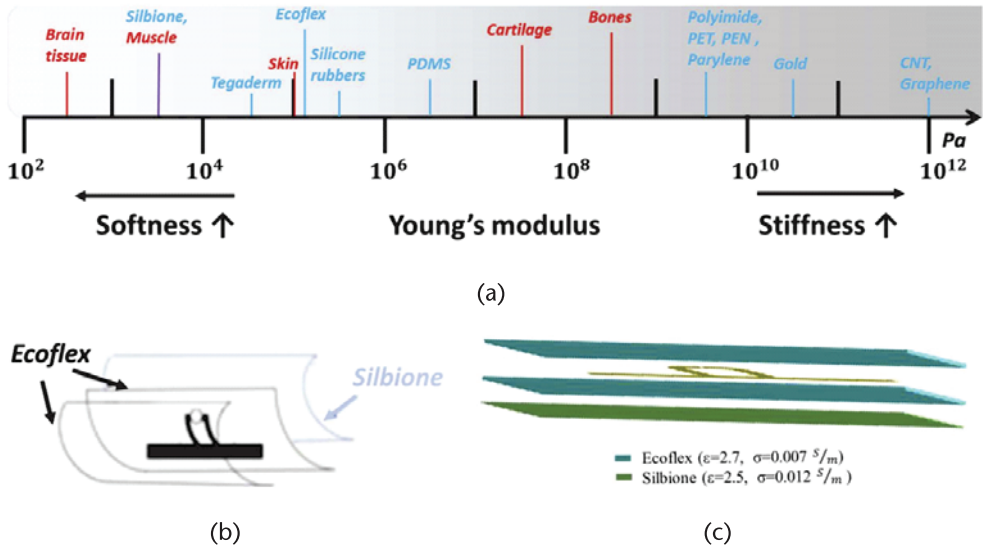

Figure 7.9 (a) Young's moduli of some human tissues (in red) and common materials used to fabricate sensors (in blue). (b) Layers of the multilayer in-silicone sensor in Figure 7.8(c). The dipole is 33 mm long. (Adapted from [29].) (c) Numerical model of the multilayer in-silicone sensor.

to be visually impaired globally in 2010 [35], and they find it challenging to recognize the objects they have to interact with.

R-FADs with temperature-sensing capabilities can provide an artificial sense for the temperature of objects to recover the thermal feeling indirectly. Moreover, self-tuning R-FADs can be designed to recognize the touched materials based on their dielectric permittivity, thus enabling the dielectric-sensing ultrability. This ultrability could be exploited for several everyday tasks, such as sensing the wetness of hair or discriminating between liquids (e.g., water and alcohol) or powders inside plastic bottles.

7.5.1 Sensing an Item's Temperature

Warm/cold sense can be restored by R-FADs embedding a temperature-sensing chip. When the sensor contacts the skin, the chip senses both the temperatures of the body and the external environment. Accordingly, a transient regime longer than 10 seconds can be experienced, depending on the object's temperature (Figure 7.10(a)). Temperature equilibrium is reached after 4 seconds (cold water at 8.8°C) to 5 seconds (hot wood at 50°C) up to 12 seconds (ice at 0°C). Consequently, depending on the difference between the starting temperature of the R-FAD sensor and the object's temperature, a variable touch duration may be needed. The thermal inertia of the actual IC embedded in the finger sensor influences the transitory duration, too. The estimation of the correct temperature can speed up by using an extrapolator. Usually, the temperature returned by the IC after the touch depends on the duration of the contact itself (Figure 7.10(b)). Denoting with Δt the contact time, and with T_∞ the actual object's temperature, then [18]

$$T_\infty = \frac{T(\Delta t) - e^{-\frac{\Delta t}{\tau}} \bullet T_0}{1 - e^{-\frac{\Delta t}{\tau}}} \tag{7.7}$$

where T_0 is the R-FAD temperature measured before the contact, τ is the time-constant depending on the thermal inertia of the considered IC. Figure 7.10(c) shows an example for some touch durations when employing the IC EM4235 by EM Microelectronic, having $\tau = 6.5$ s. When applying (7.7) to the data plotted in Figure 7.10(c), the hot water temperature was estimated. Experiments demonstrated that thanks to the extrapolator, a contact as short as a half-second long is sufficient to assess the object's temperature correctly with a ±1°C accuracy [18].

Recorded live demonstrations of temperature-sensing R-FADs exploiting (7.7) are available online regarding, in [36], continuous temperature sensing and, in [37], a real-time application. In the second video of [37] a multichannel temperature-sensing R-FAD is shown. Two sensor tags are simultaneously queried by the reader, the thumb sensor, and the index sensor. Each sensor estimates the temperature of the contacted object only based on its data.

A temperature-sensing R-FAD was tested on a sensorially impaired volunteer [16], a 45-year-old female suffering from radiotherapy-induced peripheral

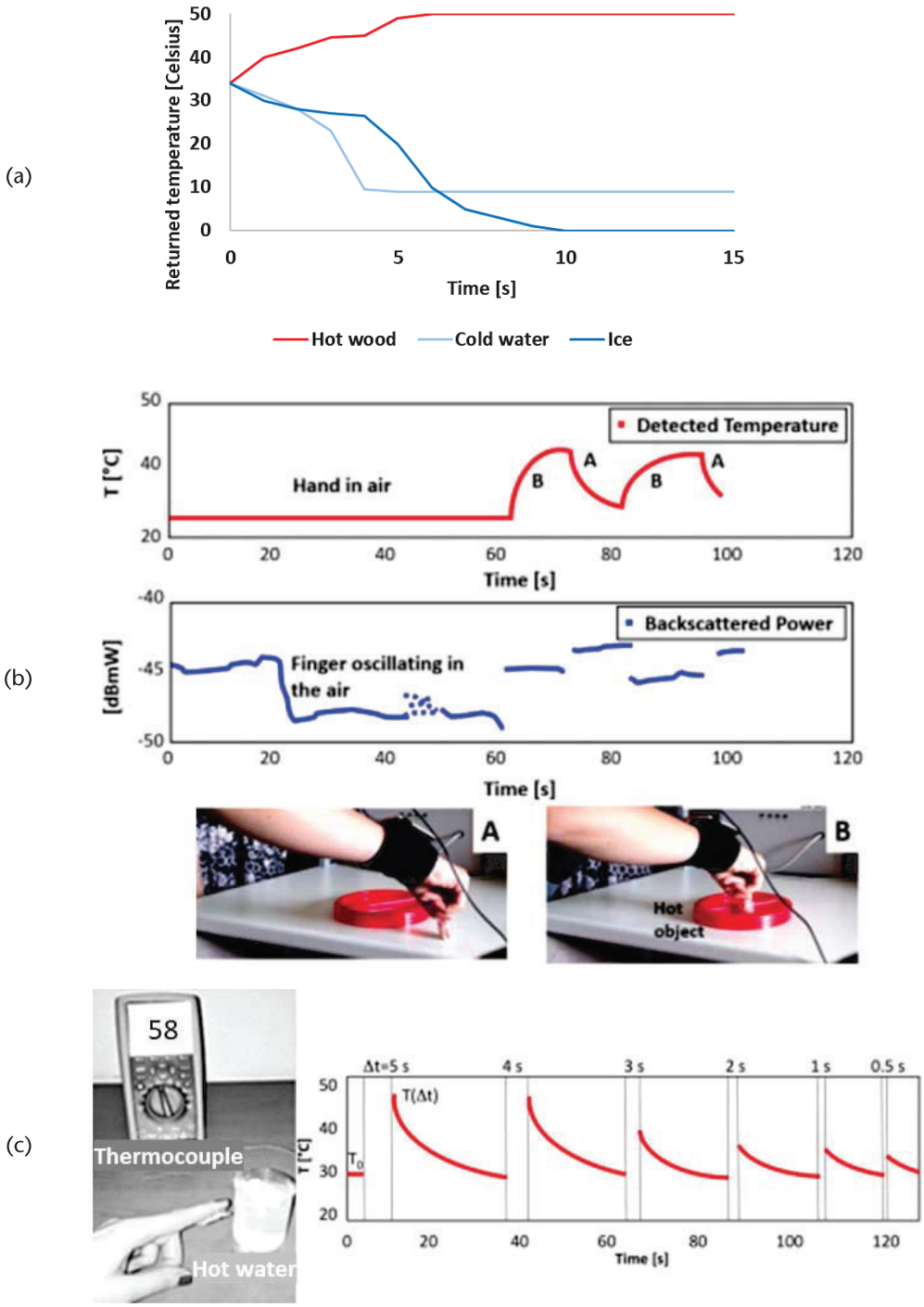

Figure 7.10 Temperature-sensing R-FADs. (a) Example of a temperature profile returned by the fingertip plaster sensor in Figure 7.8(a) embedding the Magnus-S3 IC when contacting objects. (b) Detected temperature and corresponding power backscattered by the U-tag in Figure 7.6(b) when the user cyclically touches the desk surface kept at environment temperature and a hot plastic object (approximative temperature of 40°C). (©2017 IEEE [18].) (c) Example of estimated temperature T_{∞} of a hot glass starting from the temperature recorded by the finger sensor when contacting the target objects for different time intervals. (©2017 IEEE [18].)

neuropathy from more than 5 years before the experimentation. She lost thermal perception from both upper limbs, below the elbows, and over large parts of the trunk. The temperature-sensing R-FAD was a single-sensor system, including only one plaster-sensor on the index finger. It returned visual and acoustic feedback on the temperature of the touched object. The feedback produced by a tablet consisted of a color paired with a sound. Seven color–sound couplets were selected corresponding to seven levels (i.e., ranges) of temperature between –20°C and 70°C. After 15 consecutive days of at-home training with the R-FAD through 20-minute-long sessions, the patient was able to guess the contacted objects' temperatures with remarkable accuracy (Figure 7.11). Therefore, the R-FAD was successful in restoring thermal feeling.

7.5.2 Discrimination of Materials

Dielectric-sensing R-FADs were initially proposed to aid visually impaired people in [28]. They can estimate the permittivity of the touched object by exploiting the self-tuning mechanism detailed in Section 7.3. The SC metric returned by the autotuning IC is highly sensitive to the permittivity of the touched object throughout the mismatch of the fingertip antenna that the self-tuning IC tries to compensate. The raw SC was tested to recognize different materials inside PET bottles [24, 28], to find a light switch on the wall, and to sense the filling level of a bottle (Figure 7.12(a–c)). In another test, a volunteer touched his hair before and after wetting it, and the returned raw SC was 161 and 54, respectively. However, the raw SC is affected by very significant inter- and intrasubject variabilities such as the antenna layout, the sensor positioning, adherence to human skin, the gesture performed, and the specific IC used. Therefore, the raw SC has low reproducibility and has to be carefully managed.

User-specific baseline effects can be significantly reduced by resorting to the differential SC (ΔSC), defined as the difference between the raw SC and a calibration SC value. The ΔSC was proven to discriminate dielectric contrast even lower than a single unit [39]. By exploiting the ΔSC, the intersubject variability is significantly reduced [38], whereas the intrasubject variability due to different gestures performed is still not negligible (Figure 7.12(d,e)). A live demo involving dielectric-sensing R-FAD through the ΔSC is currently available online [40].

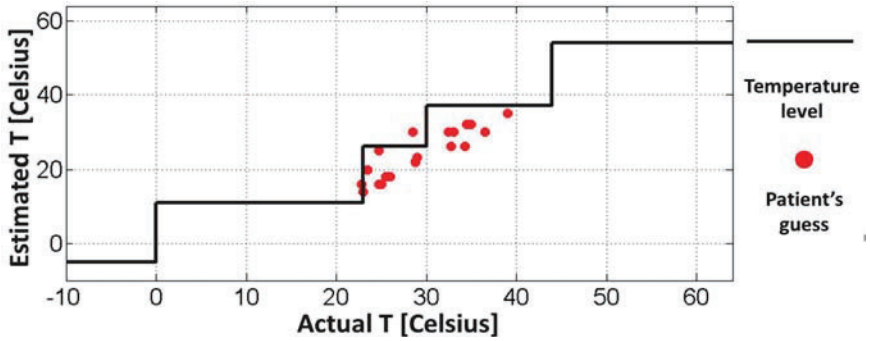

Figure 7.11 Object temperature vs. temperature estimated (red dots, one dot per touch) by a patient with thermal hypoesthesia through an R-FAD after 15 days of training. (©2019 IEEE [16].)

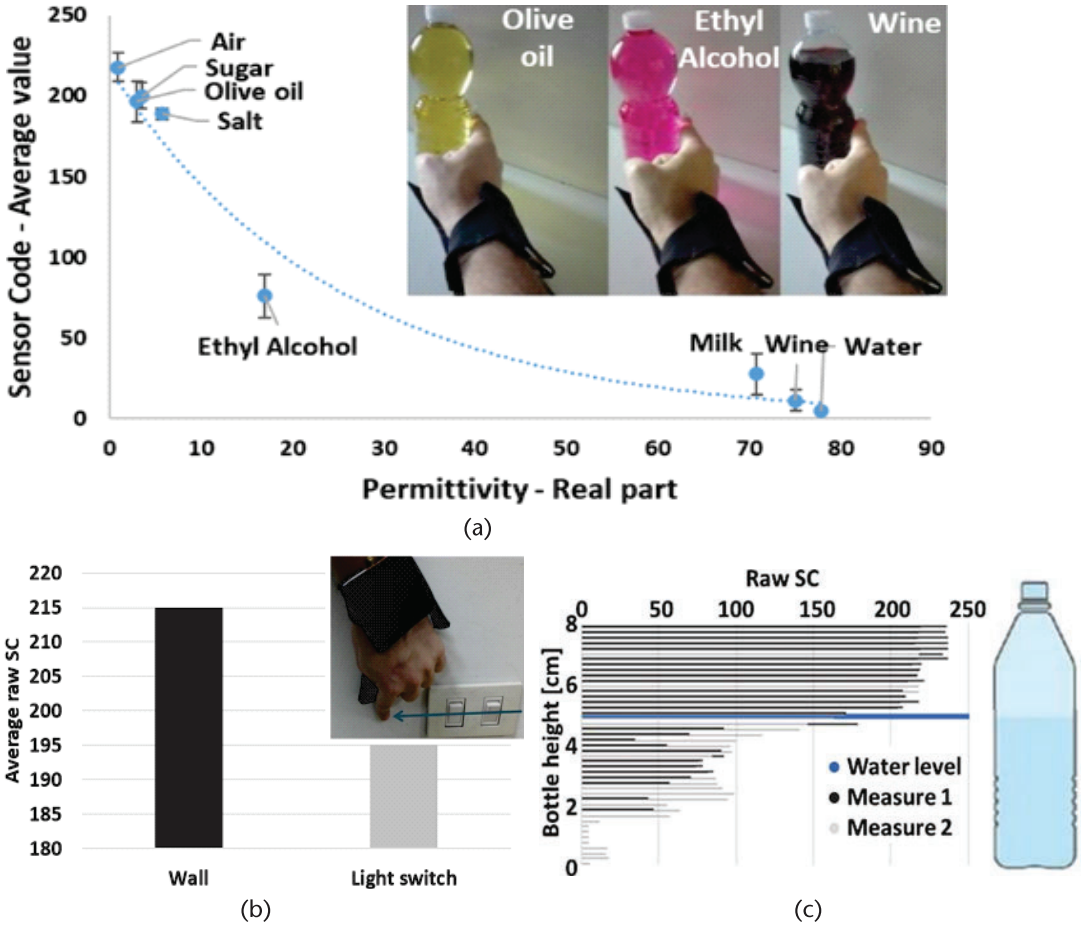

Figure 7.12 Dielectric-sensing R-FADs. (a) Mean SC value over five measurements when a single user contacts PET bottles filled with different powders or liquid. (Adapted from [28].) (b) Raw SC returned when contacting a wall and a light switch, and (c) when contacting a bottle half-filled with water twice from the top to the bottom. (d) Raw SC returned to four different users when touching nothing (air) or PET bottles filled with three liquids. (©2020 IEEE [38].) (e) Differential sensor code ΔSC corresponding to the raw SC in Figure 7.12(d) averaged on the users for two gestures. (©2020 IEEE [38].) (f) Digital fingerprints of a single user contacting three different materials, each identified by a color. (Adapted from [29].)

A further improvement on the robustness of sample data and the reliability of the identification of materials can be achieved by multichannel R-FADs, which are devices wherein all five fingers are provided with identical sensors [29]. In this case, the measurement metric is now a digital fingerprint, which is the vector of the ΔSC measured by each finger. Accordingly, when touching some materials, different digital fingerprints are observed (Figure 7.12(f)). The areas of digital fingerprints for four users and three touched objects having different permittivities are shown in Figure 7.13(a). Based on the digital fingerprints, the digital contrast can be defined as the gap of the $\overline{\Delta SC}$ (average of the returned ΔSC over all the five sensors) between two materials having different electric permittivities. The digital contrast in the case of a multichannel R-FAD achieves sensitivities up to two times those obtained by a single-sensor R-FAD using the same sensor (Figure 7.13(b)) [29].

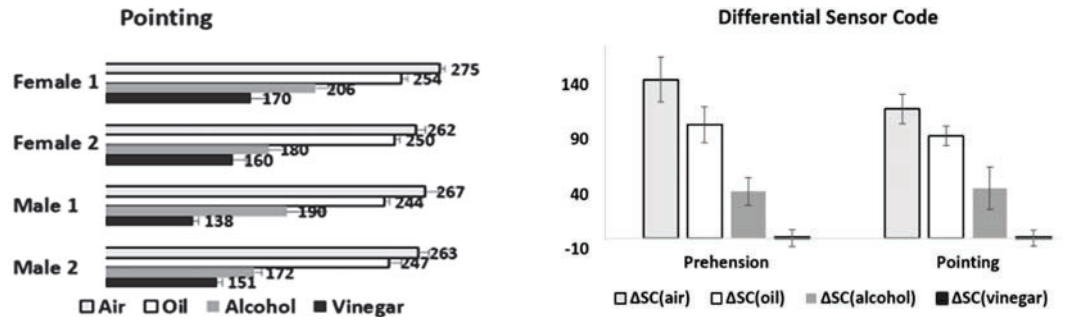

(d) (e)

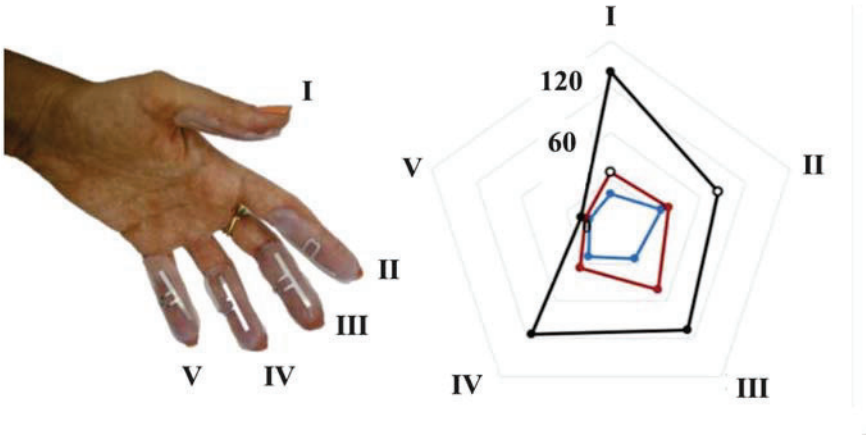

(f)

Figure 7.12 (continued)

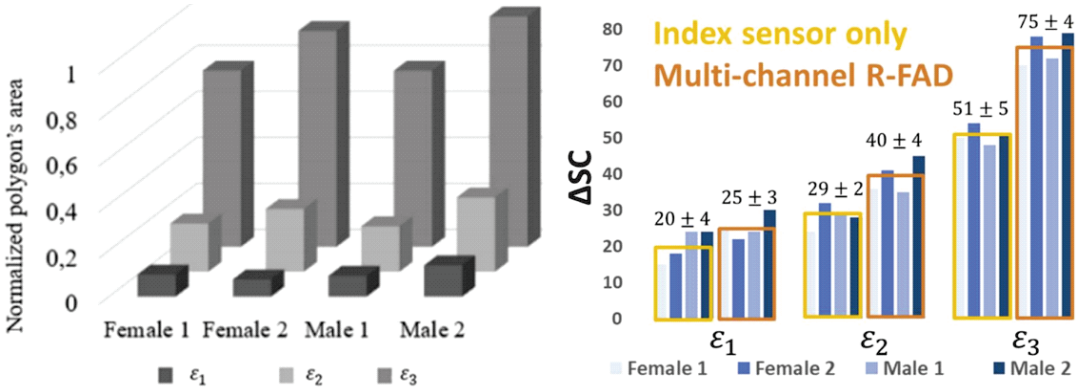

(a) (b)

Figure 7.13 Differential SCs returned by a multichannel R-FAD. (a) Areas of the digital fingerprints of four volunteers contacting three materials having different permittivities $\varepsilon_1 < \varepsilon_2 << \varepsilon_3$. (Adapted from [29].) (b) Comparison between the ΔSC returned by a single sensor and the averaged differential SC measured by a multichannel R-FAD. (Adapted from [29].)

7.6 Application to Cognitive Remapping

According to the grounded theories of cognition, physical perception is intimately related to abstract representation [41]. For example, holding a warm or cold pack was proved to influence brain activation when performing a given task [42]. Consequently, a patient suffering from a prolonged sensorial degradation will experience a significant cognitive change, losing the emotional feeling of temperature and not perceiving either warm or cold as a pleasant concept when figuring out situations.

The temperature-sensing R-FAD was employed to study the possibility of cognitive remapping caused by the above problem by resorting to the same setup: the impaired patient as in Section 7.5.1 and a group of 20 neurologically healthy volunteers (age 30±9 years). The entity of the cognitive remapping was quantified through a Stroop-like task [43], where participants are requested to name the color of ink in which color names are printed (e.g., word "red" printed in blue). Cognitive dissonance is known to delay ink naming significantly [43]. Since a comparable effect occurs for words that are not color names but imply the concept of a color (color words such as "lemon," which implies the color "yellow"), a Stroop-like effect using color words implying temperature (such as "fire," related both to "red" and "hot") was also expected. The Stroop test was completed by the control group as well as by the hypoesthesia patient. The patient was asked to perform the test before and after the R-FAD training, as detailed in Section 7.5.1. A sketch of the experiment and the results are shown in Figure 7.14. More substantial cognitive dissonances cause longer response times (RTs); theoretically, a longer RT than the sensorially impaired patient's one before the R-FAD training is expected both after the R-FAD training and in the control group. Overall, the patient's RT delay before the R-FAD training was observed for color names but not for color words (Figure 7.14(c)). The patient's RT for color words was lower than those of 66% of the control group, suggesting that the prolonged loss of the physical thermal feeling probably weakened the cognitive dissonance related to the object's temperature. Instead, after the R-FAD training, the patient's RTs were more similar to those of the control group, with higher RTs returned for color words than before the training. Accordingly, a partial recovery of the concepts of warm and cold can be inferred.

7.7 Conclusions

This chapter reviewed the state of the art of R-FADs to understand how epidermal electromagnetics can help enable the tactile internet. Establishing a reliable fingertip-wrist link is still a critical issue. This link is varied for given antenna layouts mainly because of (1) the wearer's hand form-factor, (2) the performed gesture, (3) the sensorized finger, (4) the sensor's adherence to the skin, and (5) the touched material. Partial communication insensitivity to the type of contacted object can be achieved by a constrained design of the finger antenna involving a self-tuning IC. Among the experimented manufacturing options, the in-silicone sensors are the most comfortable and practical. Lastly, applications of R-FADs for aiding sensorially impaired people and studying cognitive neural remapping were reported.

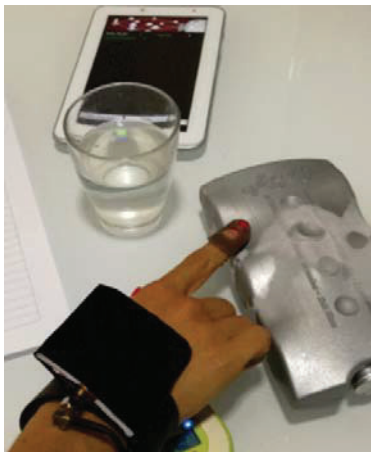

(a)

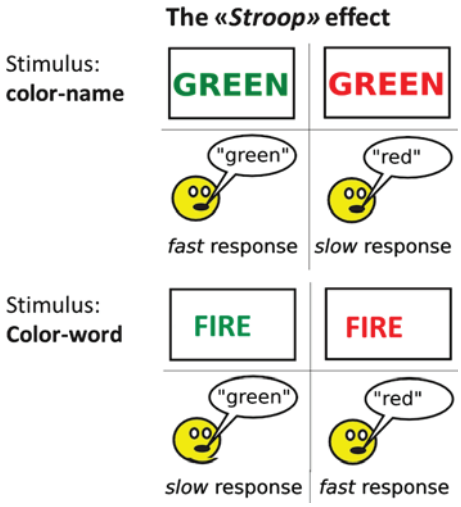

(b)

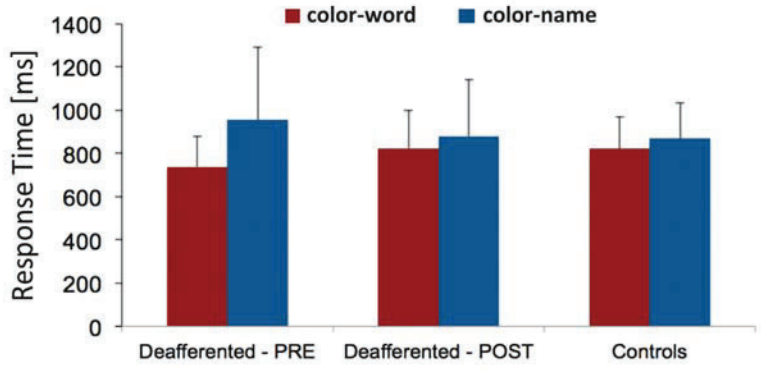

(c)

Figure 7.14 (a) Temperature-sensing R-FAD and experimental setup of R-FAD training sessions. The portable reader is connected via Bluetooth to the tablet, where an ad hoc app returns audio and visual feedback to the user. (©2019 IEEE [16].) (b) The Stroop effect and Stroop-like task. (©2019 IEEE [16].) (c) RTs of the deafferented patient before (pre) and after (post) R-FAD training are compared with those of the control group. (©2019 IEEE [16].)

R-FADs are an extremely promising technology to study the human cognitive sphere thanks to their ability to modify users' perceptions in a controlled way. According to our preliminary test, the temperature-sensing R-FAD was not only able to restore the physical thermal feeling, but also the abstract thermal feeling.

On-hand devices for enabling the TI are still little known, and future research can be envisaged. R-FADs provided with different sensing capabilities, as pressure or pH, can be included for applications such as telediagnosis; EM performance can be further enhanced by resorting to a directive wrist antenna made of the same soft-electronic technology as the fingertip sensors; and 5G R-FADs could use smart watches as readers. Moreover, cognitive remapping when conferring an ultrability to the user has never been studied and could also give helpful insight into human cognition.

7.8 Acknowledgments

The authors gratefully thank all the people in the Pervasive Electromagnetics Lab at the Tor Vergata University of Rome who worked on this topic over the years: Dr. Sara Amendola, Ms. Veronica Di Cecco, Ms. Valentina Greco, Ms. Silvia Guido, Ms. Federica Naccarata, and Ms. Cecilia Vivarelli.

References

[1] Fettweis, G. P., "The Tactile Internet: Applications and Challenges," *IEEE Vehicular Technology Magazine*, Vol. 9, No. 1, 2014, pp. 64–70.

[2] Burdea, G. C., and P. Coiffet, *Virtual Reality Technology*, Hoboken, NJ: John Wiley & Sons, 2003, "Cybersickness," pp. 269–274.

[3] Rebenitsch, L., and C. Owen, "Review on Cybersickness in Applications and Visual Displays," *Virtual Reality*, Vol. 20, No. 2, 2016, pp. 101–125.

[4] Dohler, M., et al., "Internet of Skills, Where Robotics Meets AI, 5G and the Tactile Internet," *European Conference on Networks and Communications*, Oulu, Finland, 2017.

[5] Maier, M., M. Chowdhury, B. Rimal, and D. Van, "The Tactile Internet: Vision, Recent Progress, and Open Challenges," *IEEE Communications Magazine*, Vol. 54, No. 5, 2016, pp. 138–145.

[6] Shilkrot, R. J., Huber, J. Steimle, S. Nanayakkara, and P. Maes, "Digital Digits: A Comprehensive Survey of Finger Augmentation Devices," *ACM Computing Surveys*, Vol. 40, No. 2, 2015, pp. 1–29.

[7] Su, C.- H., L. Chan, C.-T. Weng, R.-H. Liang, K.-Y. Cheng, and B.-Y. Chen, "NailDisplay: Bringing an Always-Available Visual Display to Fingertips," *Proceedings of Conference on Human Factors in Computing Systems*, Paris, France, 2013.

[8] Kao, H.- L., A. Dementyev, J. Paradiso, and C. Schmandt, "NailO: Fingernails as an Input Surface," *Proceedings of Conference on Human Factors in Computing Systems*, Seoul, Republic of Korea, 2015.

[9] Dahiya, R., "Epidermal Electronics–Flexible Electronics for Biomedical Applications," in *Handbook of Bioelectronics: Directly Interfacing Electronics and Biological Systems*, S. Carrara and K. Iniewski (eds.), Cambridge, United Kingdom: Cambridge University Press, 2015, pp. 245–255.

[10] Sedighi, P., H. Norouzi, and M. Delrobaei, "An RFID-Based Assistive Glove to Help the Visually Impaired," *IEEE Transactions on Instrumentation and Measurements*, Vol. 70, 2021, pp. 1–9.

[11] Taylor, P. S., and J. C. Batchelor, "Finger-Worn UHF Far-Field RFID Tag Antenna," *IEEE Antennas and Wireless Propagation Letters*, Vol. 18, No. 12, 2019, pp. 2513–2517.

[12] Liang, R.- H., S.-Y. Yang, and B.- Y. Chen, "InDexMo: Exploring Finger-Worn RFID Motion Tracking for Activity Recognition on Tagged Objects," *Proceedings of the 23rd International Symposium on Wearable Computers*, London, United Kingdom, 2019.

[13] Bainbridge, R. and J. A. Paradiso, "Wireless Hand Gesture Capture through Wearable Passive Tag Sensing," *2011 International Conference on Body Sensor Networks*, Dallas, TX, 2011.

[14] Amato, F., C. Occhiuzzi, and G. Marrocco, "Performances of a 3.6 GHz Epidermal Loop for Future 5G-RFID Communications," in *14th European Conference on Antennas and Propagation*, Copenhagen, Denmark, 2020.

[15] Shilkrot, R., *Digital Digits: Designing Assistive Finger Augmentation Devices*, PhD thesis, Massachusetts Institute of Technology, Cambridge, MA, 2015.

[16] Amendola, S., V. Greco, G. M. Bianco, E. Daprati, and G. Marrocco, "Application of Radio-Finger Augmented Devices to Cognitive Neural Remapping," *IEEE International Conference on RFID Technology and Applications*, Pisa, Italy, 2019.

[17] Amendola, S., V. Di Cecco, and G. Marrocco, "Numerical and Experimental Characterization of Wrist-Fingers Communication Link for RFID-Based Finger Augmented Devices," *IEEE Transactions on Antennas and Propagation*, Vol. 67, No. 1, 2019, pp. 531–540.

[18] Di Cecco, V., S. Amendola, P. P. Valentini, and G. Marrocco, "Finger-Augmented RFID System to Restore Peripheral Thermal Feeling," *IEEE International Conference on RFID*, Phoenix, AZ, 2017.

[19] Orfanidis, S., *Electromagnetic Waves and Antennas*, New Brunswick, NJ: Rutgers University Press, 2010.

[20] Bianco, G. M., S. Amendola, and G. Marrocco, "Near-Field Modeling of Self-Tuning Antennas for the Tactile Internet," *33rd General Assembly and Scientific Symposium of the International Union of Radio Science*, Rome, Italy, 2020.

[21] Amendola, S., and G. Marrocco, "Optimal Performance of Epidermal Antennas for UHF Radio Frequency Identification and Sensing," *IEEE Transactions on Antennas and Propagation*, Vol. 65, No. 2, 2017, pp. 473–481.

[22] Ferreira, D., P. Pires, R. Rodrigues, and R. F. S. Caldeirinha, "Wearable Textile Antennas: Examining the Effect of Bending on Their Performance," *IEEE Antennas and Propagation Magazine*, Vol. 59, No. 3, 2017 pp. 54–59.

[23] Caccami, M. C., and G. Marrocco, "Electromagnetic Modeling of Self-Tuning RFID Sensor Antennas in Linear and Nonlinear Regimes," *IEEE Transactions on Antennas and Propagation*, Vol. 66, No. 6, 2018, pp. 2779–2787.

[24] Bianco, G. M., S. Amendola, and G. Marrocco, "Near-Field Constrained Design for Self-Tuning UHF-RFID Antennas," *IEEE Transactions on Antennas and Propagation*, Vol. 68, No. 10, 2020, pp. 6906–6911.

[25] Marrocco, G., "The art of UHF RFID Antenna Design: Impedance-Matching and Size-Reduction Techniques," *IEEE Antennas and Propagation Magazine*, Vol. 50, No. 1, 2008, pp. 66–79.

[26] GS1, "Regulatory Status for Using RFID in the EPC Gen2 (860 to 960 MHz) Band of UHF spectrum," March 13, 2021, https://www.gs1.org/docs/epc/uhf_regulations.pdf.

[27] Amendola, S., S. Milici, G. Marrocco, and C. Occhiuzzi, "On-Skin Tunable RFID Loop Tag for Epidermal Applications," *IEEE International Symposium on Antennas and Propagation & USNC/URSI National Radio Science Meeting*, Vancouver, Canada, 2015.

[28] Bianco, G. M., and G. Marrocco, "Fingertip Self-Tuning RFID Antennas for the Discrimination of Dielectric Objects," *Proceedings of the 13th European Conference on Antennas and Propagation*, Krakow, Poland, 2019.

[29] Naccarata, F., G. M. Bianco, and G. Marrocco, "Multi-Channel Radiofrequency Finger Augmentation Device for Tactile Internet," *34th URSI General Assembly and Scientific Symposium*, Rome, Italy, 2021.

[30] Miozzi, C., G. Diotallevi, M. Cirelli, P. P. Ventini, and G. Marrocco, "Radio-mechanical Characterization of Epidermal Antennas during Human Gestures," *IEEE Sensors Journal*, Vol. 20, No. 14, 2020, pp. 7588–7594.

[31] Barrell, K., and A. G. Smith, "Peripheral Neuropathy," *Medical Clinics of North America*, Vol. 103, No. 2, 2019, pp. 383–397.

[32] Jacob, E., V. Wong Chan, C. Hodge, L. Zeltzer, D. Zurakowsy and N. F. Sethna, "Sensory and Thermal Quantitative Testing in Children with Sickle Cell Disease," *Journal of Pediatric Hematology Oncology*, Vol. 37, No. 3, 2015, pp. 185–189.

[33] Blankenburg, M., et al., "Childhood Diabetic Neuropathy: Functional Impairment and Non-Invasive Screening Assessment," *Diabetic Medicine*, Vol. 29, No. 11, 2012, pp. 1425–1432.

[34] Griffith, K. A., et al., "Evaluation of Chemotherapy-Induced Peripheral Neuropathy Using Current Perception Threshold and Clinical Evaluations," *Support Care Cancer*, Vol. 22, No. 5, 2014, pp. 1161–1169.

[35] Pascolini, D., and S. P. Mariotti, "Global Estimates of Visual Impairment: 2010," *British Journal of Ophthalmology*, Vol. 96, 2012, No. 5, pp. 614–618.

[36] Pervasive Electromagnetics Lab, *RADIOFingerTip: a Finger-Augmented-Device to Restore Peripheral Neuropathy*, Rome: Italy, University of Rome Tor Vergata, 2016, https://www.youtube.com/watch?v=DGUkYqmt-5Q&t=1s.

[37] Pervasive Electromagnetics Lab, *RadioFingerTip: Estimation of the Temperature of the Objects Touched by the Fingertip Sensor*, Rome, Italy: University of Rome Tor Vergata, 2017, https://www.youtube.com/watch?v=6quuuEiNEBs.

[38] Bianco, G. M., C. Vivarelli, S. Amendola, and G. Marrocco, "Experimentation and Calibration of Near-Field UHF Epidermal Communication for Emerging Tactile Internet," *5th International Conference on Smart and Sustainable Technologies*, Split, Croatia, 2020.

[39] Bianco, G. M., and G. Marrocco, "Sensorized Facemask with Moisture-Sensitive RFID Antenna," *IEEE Sensors Letters*, Vol. 5, 2021, No. 3, pp. 1–4.

[40] Pervasive Electromagnetics Lab, *Recognizing Materials by Touch*, Rome, Italy: University of Rome Tor Vergata, 2020, https://www.youtube.com/watch?v=bQZOG3eVgm0.

[41] Barsalou, L. W., "Grounded Cognition: Past, Present, and Future," *Topics in Cognitive Science*, Vol. 2, No. 4, 2010, pp. 716–724.

[42] Kang, Y., L. E. Williams, M. S. Clark, J. R. Gray, and J. A. Bargh, "Physical Temperature Effects on Trust Behavior: The Role of Insula," *Social Cognitive and Affective Neuroscience*, Vol. 6, No. 4, 2011, pp. 507–511.

[43] MacLeod, C. M., "Half a Century of Research on the Stroop Effect: An Integrative Review," *Psychological Bulletin*, Vol. 109, No. 2, 1991 pp. 163–203.